10-1-2022

Guidelines for Fabricating Highly Efficient Perovskite Solar Cells with Cu2O as the Hole Transport Material

Sajid Sajid
United Arab Emirates University

Salem Alzahmi
United Arab Emirates University

Imen Ben Salem
Zayed University

Ihab M. Obaidat
United Arab Emirates University

Article

Guidelines for Fabricating Highly Efficient Perovskite Solar Cells with Cu$_2$O as the Hole Transport Material

Sajid Sajid [1,2], Salem Alzahmi [1,2,*], Imen Ben Salem [3] and Ihab M. Obaidat [2,4,*]

1 Department of Chemical & Petroleum Engineering, United Arab Emirates University, Al Ain P.O. Box 15551, United Arab Emirates
2 National Water and Energy Center, United Arab Emirates University, Al Ain P.O. Box 15551, United Arab Emirates
3 College of Natural and Health Sciences, Zayed University, Abu Dhabi P.O. Box 144534, United Arab Emirates
4 Department of Physics, United Arab Emirates University, Al Ain P.O. Box 15551, United Arab Emirates
* Correspondence: s.alzahmi@uaeu.ac.ae (S.A.); iobaidat@uaeu.ac.ae (I.M.O.)

Abstract: Organic hole transport materials (HTMs) have been frequently used to achieve high power conversion efficiencies (PCEs) in regular perovskite solar cells (PSCs). However, organic HTMs or their ingredients are costly and time-consuming to manufacture. Therefore, one of the hottest research topics in this area has been the quest for an efficient and economical inorganic HTM in PSCs. To promote efficient charge extraction and, hence, improve overall efficiency, it is crucial to look into the desirable properties of inorganic HTMs. In this context, a simulation investigation using a solar cell capacitance simulator (SCAPS) was carried out on the performance of regular PSCs using inorganic HTMs. Several inorganic HTMs, such as nickel oxide (NiO), cuprous oxide (Cu$_2$O), copper iodide (CuI), and cuprous thiocyanate (CuSCN), were incorporated in PSCs to explore matching HTMs that could add to the improvement in PCE. The simulation results revealed that Cu$_2$O stood out as the best alternative, with electron affinity, hole mobility, and acceptor density around 3.2 eV, 60 cm^{2}V^{-1}s^{-1}, and 10^{18} cm^{-3}, respectively. Additionally, the results showed that a back electrode with high work-function was required to establish a reduced barrier Ohmic and Schottky contact, which resulted in efficient charge collection. In the simulation findings, Cu$_2$O-based PSCs with an efficiency of more than 25% under optimal conditions were identified as the best alternative for other counterparts. This research offers guidelines for constructing highly efficient PSCs with inorganic HTMs.

Keywords: numerical simulation; inorganic charge-transporting layer; performance optimization; perovskite solar cell

1. Introduction

Perovskite solar cells (PSCs) utilizing organic–inorganic halide perovskites have been realized as emerging solar cells, with rapidly progressing power conversion efficiencies (PCEs), ease of processing, and relatively low-cost production, among other photovoltaics [1,2]. The first use of organic–inorganic halide perovskites was reported in dye-sensitizer solar cells with a PCE of 3.9% in 2009, which was a huge achievement in the field of excitonic solar cells [3]. Following that, perovskite quantum dots were utilized in PSCs, which had a 6.5% PCE with low stability due to liquid electrolytes [4]. Then, 2,2′,7,7′-Tetrakis[N,N-di(4-methoxyphenyl)amino]-9,9′-spirobifluorene (spiro-OMeTAD) was used as a hole transport material (HTM), which increased the stability of PSCs in 2012, achieving a PCE of 9.1% [5]. The PCE of PSCs was improved further by modifying the halide mixture, deposition techniques, and HTMs in organic–inorganic halide perovskites, resulting in a PCE of 22.1% in 2016. Subsequently, most of the PSCs with significant increases in PCE over 25% have been reported with organic HTMs [6]. High-performance organic HTMs, however, are frequently made of costly organic conjugated molecules, such

as spiro-OMeTAD or semiconductor polymers [7,8], which restricts their potential to be manufactured at a large scale and at a reasonable cost [9–12]. In addition, hygroscopic additives, such as lithium or cobalt salts, are frequently needed to improve their hole mobilities and appropriate Fermi level alignment, resulting in device instability through water-assisted photoactive material degradation [9,13].

In this context, alternatives such as NiO, Cu_2O, CuI, CuSCN, molybdenum trioxide (MoO_3), and copper zinc tin sulfide ($CuZnSnS_2$) have emerged as low-cost, highly conductive, stable, and dopant-free HTMs [14–20]. Furthermore, the energy levels of inorganic HTMs are remarkably similar to perovskite's frontier energy levels. MoO_3 HTMs employed in PSCs displayed a high open-circuit voltage (V_{oc}) of 1.15 V [21]. Then, the use of NiO HTM attained a PCE of 7.6% [22]. Because of the lower fill factor (FF), the performance of NiO-based PSCs was still inferior to that of organic HTMs due to the low conductivity feature of NiO. Inorganic CuO HTMs were further investigated as an alternative to organic HTMs and attained a PCE of 19.0% in PSCs with good stability [23]. The PCEs of inverted PSCs using inorganic HTMs have been reported to be around 10%; however, this figure has lately risen to more than 20% [24]. There is still a significant difference between the PCEs of PSCs in particular regular design-employing inorganic HTMs and their organic counterparts. Hence, it is critical to examine the factors that influence PSC performance.

Nevertheless, due to perovskite's incompatibility with a variety of chemical precursors and deposition techniques, research has primarily focused on inverted structures of PSCs using inorganic HTMs. Thus far, very few investigations have looked into inorganic HTMs that can be used for cost-effective regular PSC architectures [25,26]. The use of copper derivatives (copper sulfide (CuS), copper chromium oxide ($CuCrO_2$), and Cu_2O) in regular PSCs has showcased potential deposition techniques of inorganic HTMs [27–29]. Cu_2O has recently been used as an HTM in the regular design of PSCs, which has resulted in PCEs of 17% to 18%, demonstrating the potential of this HTM for further PCE enhancement [29,30]. In this context, theoretical studies are just as vital as experimental ones [31,32]. Therefore, a simulation study is conducted to provide guidelines for taking into account crucial requirements for producing highly efficient regular PSCs based on Cu_2O as HTMs. With the help of simulations and optimization, a 25.2% PCE of Cu_2O-based PSCs is produced under optimal conditions. When fabricating PSCs using inorganic HTMs, the simulation findings imply that electron affinity, hole mobility, acceptor density, and metal work function should all be considered.

2. Simulation Parameters and Computational Details

Simulation methods can help explain the phenomena existing in solar cells [33–37]. In order to gain a better understanding, a theoretical study using SCAPS software was conducted. A planar PSC configuration ($FTO/TiO_2/MAPbI_2Br/HTM/Au$) was simulated as a baseline to evaluate the impact of our method, as depicted in Figure 1a,b. The basic physical parameters for the simulation are listed in the Table 1. Most of them were chosen from recent publications [38–40]. The solar radiation spectrum of AM1.5G was used in this simulation as a light source. The light reflection was set to 0 and 1 for the top and bottom contacts, respectively. With a Gaussian energy distribution, defects in the energy levels were considered in the middle of their characteristic energy bandgap of 0.1 eV in the simulated thin films.
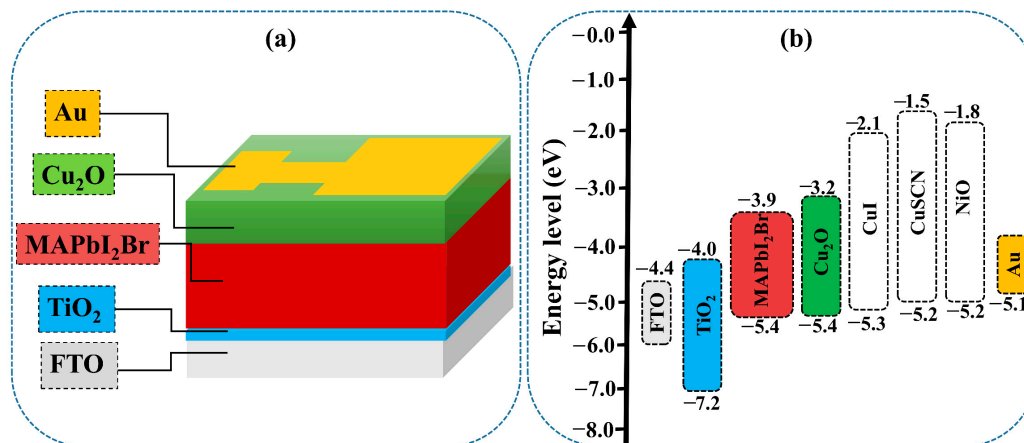
Figure 1. Schematic illustration of the as-simulated devices (**a**) and energy band diagram of the used materials (**b**).

Modeling techniques define fundamental phenomena in photovoltaic devices, which allows for the instinctive classification of optimized operating conditions for each parameter [41]. For further practical applications of heterojunction solar cells, SCAPS is ideal for intraband tunneling and trap-assisted tunneling [42]. The strength of this modeling technique was initially simulated using various inorganic HTMs in the PSCs, and later, the results were compared with experimental results [30,39]. For holes and electrons, capture cross-sections were set to 10–16 cm^2, which resulted in perovskites having carrier diffusion lengths of approximately 1 μm [43]. Active layer thickness was set to 400 nm in order to provide the efficient collection of charges. The recombination rate of the bimolecular electron-hole has a tremendous effect on the solar cell efficiency, so the total recombination in the as-simulated PSCs was taken into account by SCAPS. SCAPS software does not take into account the recombination of charges at the corresponding interfaces. Therefore, two thin defect layers were stacked at the HTM–perovskite and electron transport material (ETM)–perovskite interfaces to overcome the interfacial defect density, as presented in Table 2. This structure allowed for the evaluation of the role of interface adjustment in the simulated and experimental effects in determining the device efficiency [44,45].

Table 1. Basic parameters of the materials used for as-simulated PSCs.

Parameters/Units	TiO$_2$ [46]	MAPbI$_2$Br [47–49]	CuSCN [50]	CuI [51,52]	Cu$_2$O [53]	NiO [11]
Thickness/nm	30	400	80	80	80	80
Defects/cm^3	10^{17}	10^{17}	10^{17}	10^{17}	10^{17}	10^{17}
Band gap/eV	3.2	1.8	3.4	3.1	2.17	3.6
Electron affinity/eV	4.0	3.93	1.7	2.1	3.2	1.46
Dielectric constant	100	25	10	6.5	6.6	11.2
Effective valence band density/cm^{-3}	2×10^{20}	3×10^{18}	2.5×10^{19}	2.5×10^{19}	2.5×10^{19}	2.5×10^{19}
Effective conduction band density/cm^{-3}	10^{21}	4×10^{18}	1.5×10^{18}	1.5×10^{18}	1.5×10^{18}	1.5×10^{18}
Electron mobility/cm$^2 \cdot$V$^{-1} \cdot$s^{-1}	0.006	15	0.0002 [54]	1.5 [12]	0.02 [55]	1.4
Holemobility/cm$^2 \cdot$V$^{-1} \cdot$s^{-1}	0.003	15	0.2 [54]	4.8 [12]	90 [52,55]	4.9
Donor concentration/cm^{-3}	5×10^{19}	1×10^{18}	0	0	0	0
Acceptor concentration/cm^{-3}	0	1×10^{18}	3×10^{18}	3×10^{18}	3×10^{18}	3×10^{18}

Table 2. Basic parameters for defect layers at the interfaces of ETM–perovskite and HTM–perovskite [11,12,56].

Parameters and Units	ETM–Perovskite	HTM–Perovskite
Dielectric constant	30	6.6
Band gap/eV	1.8	2.17
Electron affinity/eV	3.93	3.2
Thickness/μm	0.002	0.002
Electron and hole mobility/$cm^2 \cdot V^{-1} \cdot s^{-1}$	50, 50	0.5, 0.5
Acceptor concentration/cm^{-3}	0	2×10^{17}
Donor concentration/cm^{-3}	2.14×10^{17}	0
Effective conduction band density/cm^{-3}	2.5×10^{20}	2×10^{17}
Effective valence band density/cm^{-3}	2.5×10^{20}	1.1×10^{19}
Characteristic energy for donor- and acceptor-like tails/eV	0.015, 0.015	0.01, 0.01
Band tail density of states/$cm^{-3}eV^{-1}$	1×10^{14}	1×10^{14}
Capture cross-section for electrons and holes in donor tail states/cm^2	1×10^{-15}, 1×10^{-17}	1×10^{-15}, 1×10^{-17}
Capture cross-section for electrons and holes in acceptor tail states/cm^2	1×10^{-17}, 1×10^{-15}	1×10^{-17}, 1×10^{-15}
Switch-over energy/eV	0.7	0.8
Density of mid-gap acceptor- and donor-like state/$cm^{-3}eV^{-1}$	1×10^{16} to 1×10^{19}	1×10^{17} to 1×10^{19}
Capture cross-section of electrons and holes in donor mid-gap states/cm^2	1×10^{-17}, 1×10^{-18}	1×10^{-16}, 1×10^{-17}
Capture cross-section of electrons and holes in acceptor mid-gap states/cm^2	1×10^{-18}, 1×10^{-17}	1×10^{-17}, 1×10^{-16}

3. Results and Discussion

3.1. Identifying the Best HTM

In order to identify the best HTM for efficient PSCs, the photovoltaic parameters with different HTMs, such as NiO, Cu_2O, CuI, and CuSCN, were simulated. The schematic diagram of the simulated devices and the energy band diagrams are given in Figure 1a,b. The basic parameters of the used materials are given in Table 1. While modeling for various HTMs, the parameters of the ETM and perovskite layers were fixed. Additionally, the same values for both bulk and interface defect densities were used to maintain a consistent analysis.

The current–voltage (J-V) characteristic curves and external quantum efficiency (EQE) of the as-simulated PSCs are depicted in Figure 2a,b, respectively. The photovoltaic metrics of the as-simulated devices are presented in Table 3. The simulation results showed that, when the HTM parameters (mentioned in Table 1) were altered, the photovoltaic metrics varied, particularly the Voc and fill factor (FF), as shown in Figure 2a and Table 2. Furthermore, it can be seen from Figure 2b that there was a little variance in the EQEs of the as-simulated PSCs. From the simulation results, it was noticed that the PSC with the Cu_2O HTM delivered a higher performance compared to the other HTMs. The superior performance of the Cu_2O-based PSC was attributed to the alignment of frontier energy levels, suitable electron affinity, and hole mobility of the as-simulated materials, as discussed below. Additionally, the simulation results closely match the experimental findings of previous published research [29,30].
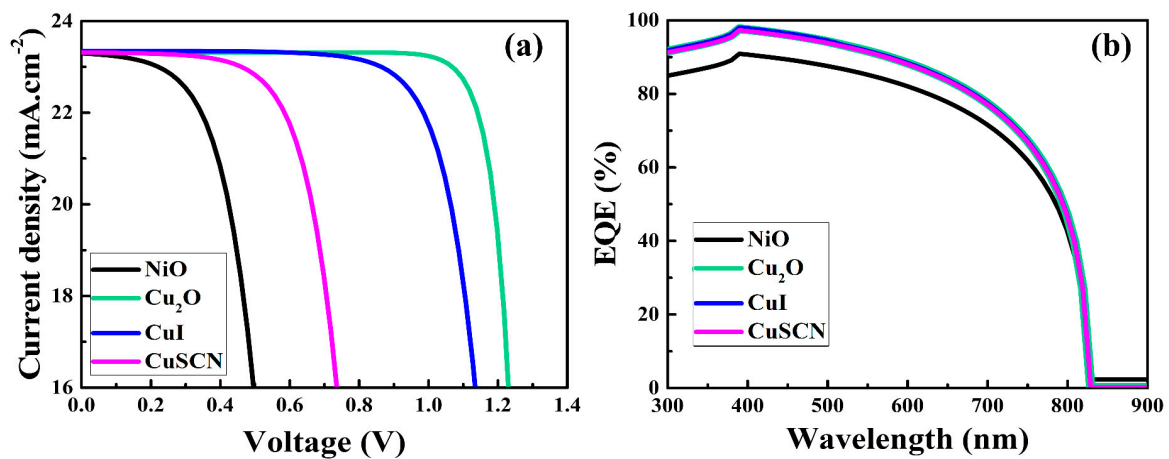
Figure 2. The J-V curves (**a**) and EQEs (**b**) of the as-simulated PSCs.

Table 3. Photovoltaic parameters obtained from the simulation of PSCs with different HTMs.

Parameters	NiO	Cu$_2$O	CuI	CuSCN
V_{oc} (V)	0.720859	1.292878	1.138577	0.956405
J_{sc} (mA·cm^{-2})	23.28859840	23.30958402	23.33917732	23.30569402
FF (%)	50.8580	83.6563	72.0141	59.9157
PCE (%)	8.5379	25.2110	21.8071	13.3550

For the efficient flow of electrons from perovskite to the ETM, the conduction band of the ETM should align with the perovskite's conduction band [57,58]. It is also essential that the valance band of the HTM match with the absorber layer in order to facilitate the transport of holes between them [59,60]. In other words, this can increase the built-in potential, which is critical for improving the V$_{oc}$ values of the PSCs. To observe the energy band matching between HTMs and the perovskite layer, the energy band levels of the as-simulated PSCs were analyzed, as shown in Figure 3. It can be seen from the energy levels of the as-simulated PSCs that there was a formation of an energy barrier in the cases of the NiO, CuI, and CuSCN HTMs. This energy barrier hindered the transportation of holes from the perovskite layer to the HTM, and as a result, the performances of the PSCs dropped. Energy barriers with values of −0.48 eV, −0.40 eV, −0.21 eV, and −0.11 eV were calculated for NiO, CuSCN, CuI, and Cu$_2$O, respectively. Since NiO had the highest energy barrier, therefore the lowest V$_{oc}$ of 0.72 V and lowest PCE of 8.5% were obtained. On the other hand, the Cu$_2$O HTM had the lowest energy barrier of −0.11 eV to the flow of holes, and thus, the PSC delivered the highest PCE of 25.2%. With regard to the low energy barrier resulting from frontier energy level alignment with the perovskite layer, Cu$_2$O had a superior performance. Cu$_2$O was, therefore, regarded as the best HTM for usage in the PSCs. In the following sections, we examine and analyze various factors of Cu$_2$O that affect the performance of PSCs.
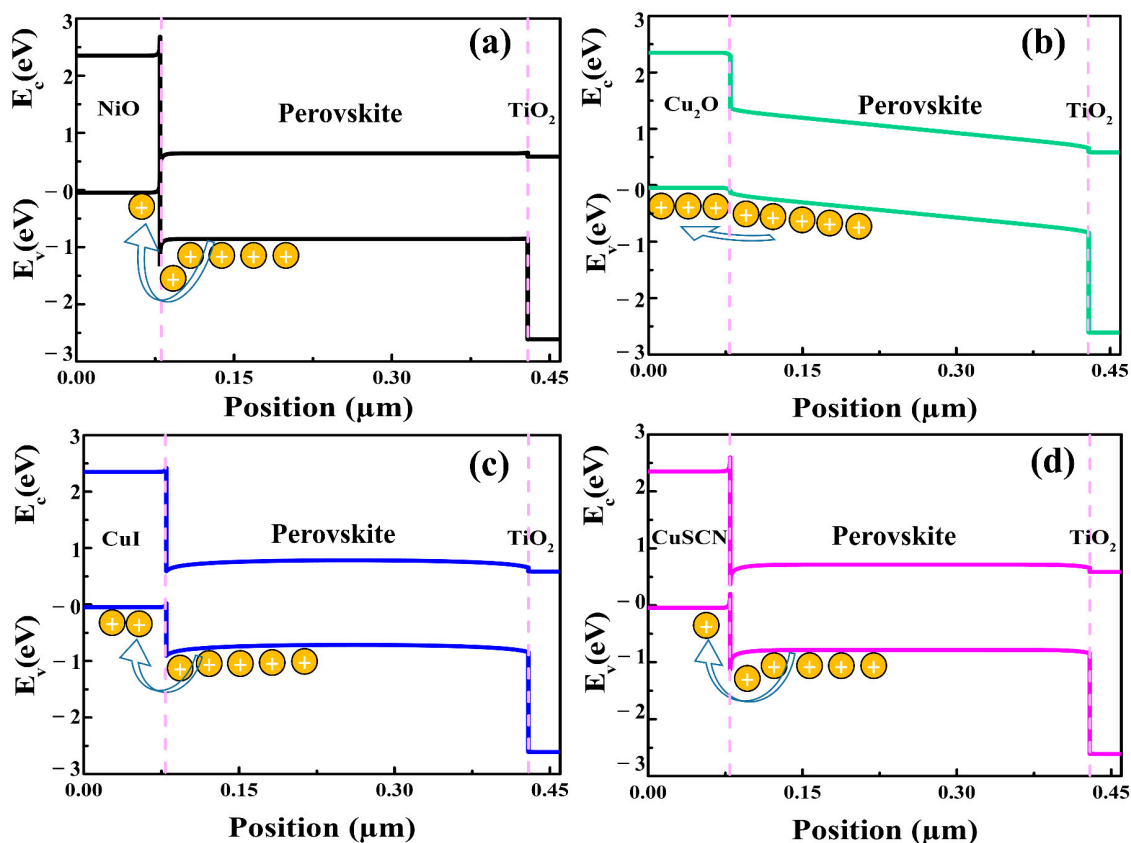
Figure 3. Energy band diagrams of the as-simulated PSCs with indication of energy barriers at the interfaces of different HTMs and the perovskite layer. NiO/perovskite (**a**), Cu$_2$O/perovskite (**b**), CuI/perovskite (**c**), and CuSCN/perovskite (**d**).

3.2. Electron Affinity of Cu$_2$O and PSC Performance

The PCE of a PSC can be improved by ensuring that the HTM and perovskite layer are aligned in terms of frontier energy levels. In this context, the valence energy band (E$_v$) must be taken into account in order to understand this difference between the HTM and the perovskite layer. The mismatching between the E$_v$ of perovskite and an HTM is generally denoted by valance band offset (VBO), which can be determined by the electron affinities of the corresponding materials. In addition, if the VBO between the HTM and perovskite layer is small, the performance of the PSC is superior compared to higher values of VBO. In the simulation, it was observed that the electron affinity of Cu$_2$O had a significant impact on the performance of PSCs. There were essentially no differences in the patterns of photovoltaic parameters with varied electron affinities of HTM from those reported in a previous work [61]. In order to obtain the optimal value for the electron affinity of Cu$_2$O, the affinity was varied from 1.5 eV to 3.7 eV, as depicted in Figure 4a,b. The major impacts obtained were on the V$_{oc}$ and FF values of the PSCs. The V$_{oc}$ and FF values were improved substantially when the affinity was changed from 2.0 eV to 3.2 eV. Correspondingly, the PCE was boosted from 19.6% to 25.2%.
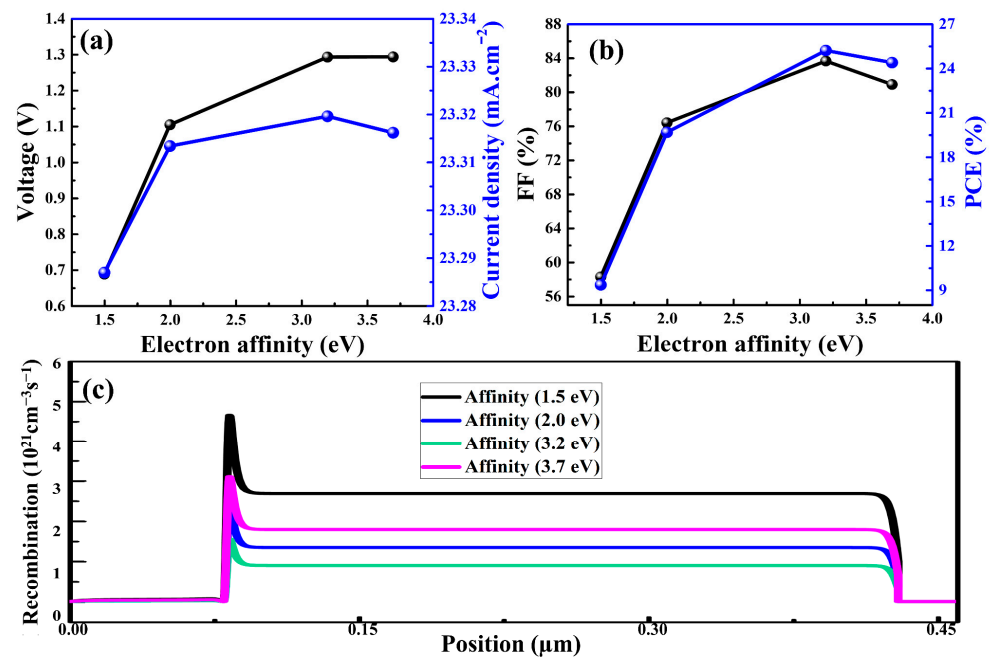
Figure 4. Photovoltaic parameters (**a**,**b**) and charge carrier recombination rates (**c**) of the as-simulated PSCs as a function of electron affinity of Cu_2O.

The simulation results revealed that high or low values of electron affinity resulted in inferior device performance, which was due to mismatch the in E_v levels of HTM and perovskite. In order to achieve the highest PCE, we assumed that the optimal electron affinity for Cu_2O was 3.2 eV, and that for perovskite was 3.93 eV. Furthermore, aligning the frontier energy levels was desirable to reduce the recombination rate at the interface between Cu_2O and perovskite, as shown in Figure 4c. Consequently, the PCEs of the PSCs could be improved by manipulating the E_v of the HTM relative to the perovskite layer.

3.3. Hole Mobility of Cu_2O and PSC Performance

Since the HTM is responsible for collecting and transporting holes from the perovskite layer to the back electrode, the hole mobility (μ_h) of the used HTM should be high enough to transport holes before they recombine. An optimum value of hole mobility up to 90 $cm^2V^{-1}s^{-1}$ for Cu_2O was considered from the previous literature [61]. However, the μ_h of Cu_2O was adjusted from 20 to 100 $cm^2V^{-1}s^{-1}$ to examine the effect on the performance of the PSCs. The J-V curves and PCEs of the as-simulated PSCs as a function of the hole mobility of Cu_2O are depicted in Figure 5. It can be seen that the short-current density (J_{sc}) remained nearly constant, whereas the FF and V_{oc} improved as the μ_h of Cu_2O was increased. Because of the improvement in hole conduction across the Cu_2O HTM, the PCE increased from 15.4% to 25.2% when the μ_h was increased from 20 to 100 $cm^2V^{-1}s^{-1}$. The improvement in PCE could be attributed to the high μ_h that reduced the series resistance within the PSCs [62]. It should be noted that the simulation results showed almost no changes in the PCEs for μ_h from 60 to 100 $cm^2V^{-1}s^{-1}$, which is consistent with previous results [63,64]. The simulation results suggested that the optimal value of μ_h that corresponded to the highest PCEs was in the range from 60 to 100 $cm^2V^{-1}s^{-1}$. These results provide guidelines for the optimization of PSC performance by adjusting the hole mobilities of HTMs.
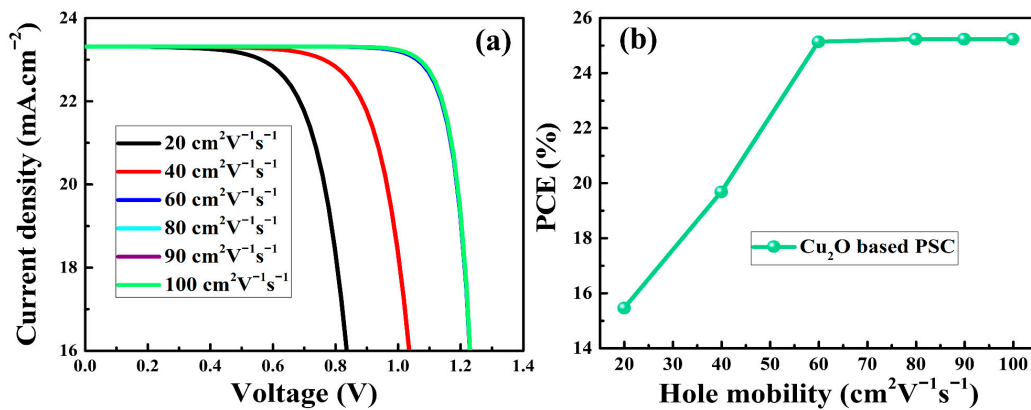
Figure 5. The J-V curves (**a**) and PCE (**b**) of the as-simulated PSCs as a function of hole mobility of Cu$_2$O HTM.

3.4. Acceptor Density of Cu$_2$O and PSC Performance

It was reported that p-type doping of an HTM produced more positive charges (majority charge carriers) and, thus, improved the bulk conductivity of the HTM and the performance of the PSCs [35]. Majority charge carriers that can be created at suitable acceptor densities (N$_a$) can greatly boost the photovoltaic parameters of PSCs. When using PSCs, an iterative approach of doping concentration aids in the improvement of their overall performance [65]. In order to understand the influence of N$_a$ on the performance of PSCs, the N$_a$ values were changed from 10^7 to 10^{18} cm^{-3} in the Cu$_2$O. As a function of the N$_a$ values of Cu$_2$O, the J-V curves, V$_{oc}$, FF, and PCE of the as-simulated devices are presented in Figure 6a–c, respectively. As the N$_a$ of Cu$_2$O increased, the V$_{oc}$ increased from 1.13 to 1.29 V. It was the rise in the built-in electric potential at the Cu$_2$O–perovskite interface that was responsible for the greater values of V$_{oc}$ observed at higher N$_a$ values. The FF and PCE increased from 76.6 to 83.6% and 20.2 to 25.2%, respectively, with the increase in N$_a$ of Cu$_2$O. The larger N$_a$ value raised the electric potential, and therefore, the built-in electric field at the interface of the perovskite and HTM increased. The built-in electric field promoted the oriented charge carrier transportation and, thus, minimized the recombination losses [66]. In addition, the reduced recombination rate of charge carriers boosted the PCE of the PSCs by reinforcing the separation of charge carriers. From the simulations, the optimal value for N$_a$, which resulted in the highest PCE, was 10^{18} cm^{-3}. This optimal N$_a$ value of Cu$_2$O is consistent with earlier reports [47]. This was attributed to shallow coulomb traps, which increased the hole mobility of Cu$_2$O.
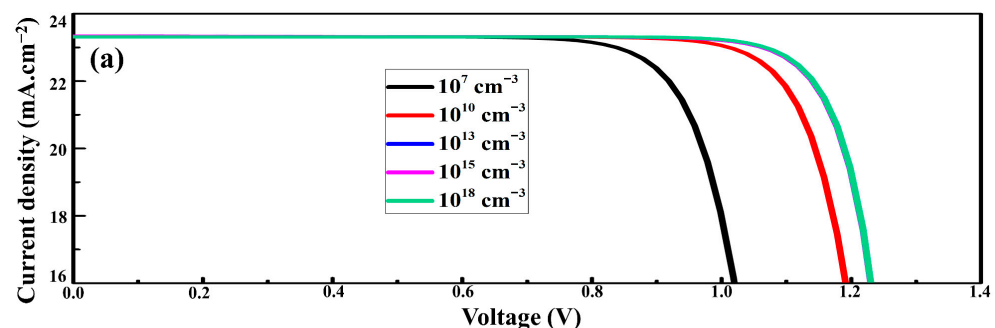

Figure 6. *Cont.*
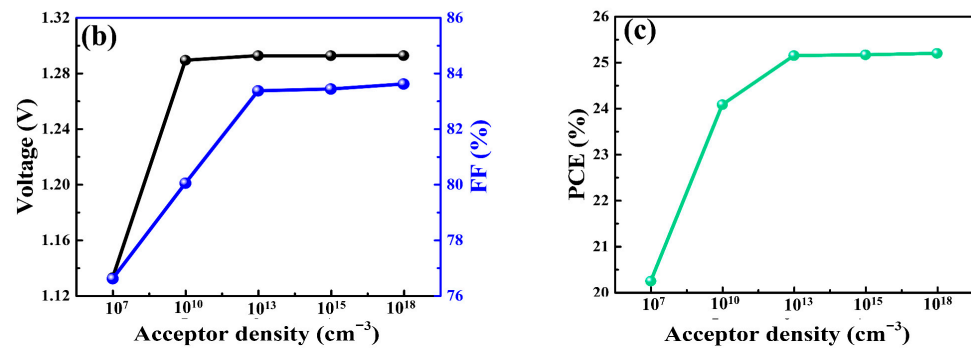
Figure 6. The J-V curves (**a**), V_{oc}, FF (**b**), and PCE (**c**) of the as-simulated PSCs.

3.5. Contact of Back Electrode with Cu_2O and PSC Performance

Because the Cu_2O layer was placed on top of the perovskite and the back electrode made contact with this HTM, it was critical to explore charge carrier transport when Ohmic or Schottky formations occurred, as these could alter charge collection [67]. The proper collection of holes through the back electrode requires the establishment of an Ohmic or Schottky contact with a small barrier. In this context, various metal electrodes, such as Ag, Cu, and Au with work functions of 4.74 eV, 4.90 eV, and 5.10 eV, respectively, were integrated in the as-simulated PSCs. It was revealed that the performance of the PSCs was affected by varying the work function value, as can be seen in Figure 7. In the presence of variable work function, the obtained behaviors of V_{oc}, FF, and PCE matched those reported in previously published research [67]. It was revealed that a metal electrode with high work function resulted in an improved V_{oc} of 1.29 V. Furthermore, the FF climbed to a maximum value of 83.65% with rising work function. Due to the improved built-in voltage, the V_{oc} increased as the work function of the metal electrode increased. For the work function value of 5.1 eV, the PCE improved, reaching a maximum value of 25.21%. The improvement in the performance of PSCs could be attributed to the small series resistance resulting from a decrease in the Schottky barrier at the interfaces of Cu_2O–HTM and Au–electrode. In Figure 7b,c, it is shown that Schottky barriers were formed in the energy band diagram for the work functions of electrodes of 4.74 eV and 4.90 eV, respectively. In Figure 7d, a Schottky barrier for holes was significantly reduced when the work function was equal to or smaller than the valence energy band of the HTM [68], resulting in a significant enhancement in the efficiency of PSCs. The findings of the simulation showed that Cu_2O could be utilized in the PSCs, but the deposition of inorganic HTMs in the regular designs of PSCs should also be taken into consideration. For instance, inorganic HTMs are challenging to dissolve in the non-polar solvents needed to preserve the perovskite layer. In this regard, surfactant modifications [29] or chemical solvents, such as dipropyl sulfide [30] and isopropanol suspension [69], that are less aggressive to the degradation of the perovskite layer might be used to deposit solution-processed inorganic HTMs in regular PSCs.
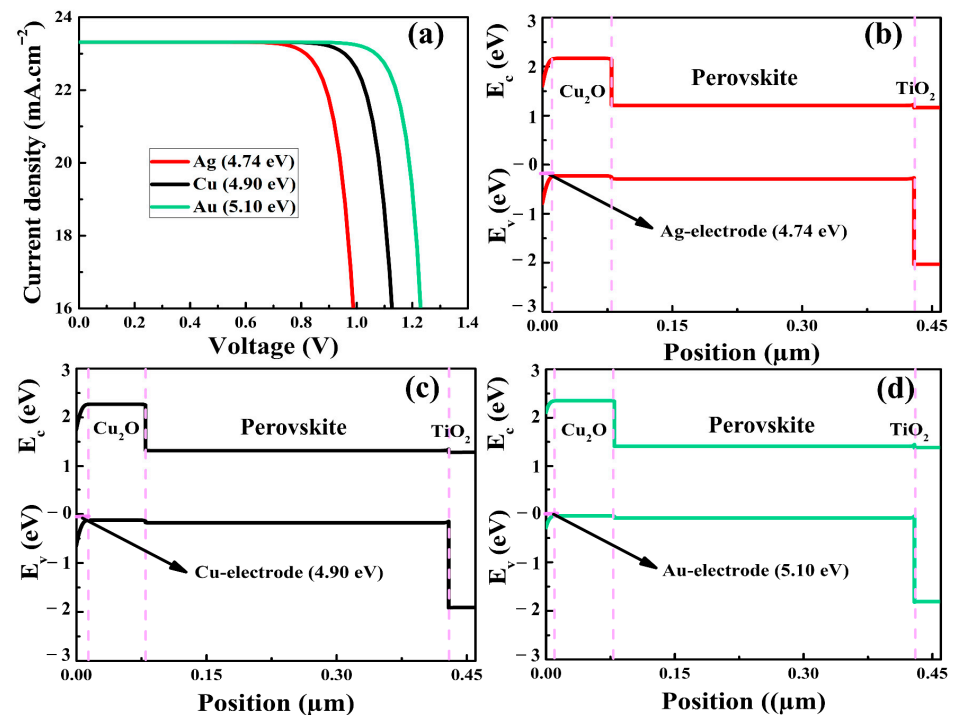
Figure 7. The J-V curves (**a**) and energy band alignments (**b–d**) of the as-simulated PSCs as a function of back electrode work function.

4. Conclusions

A numerical analysis was performed to find the optimum conditions for PSCs with inorganic HTMs. Several factors that could affect the performance of PSCs were thoroughly investigated. According to the simulation results, the optimal electron affinity, hole mobility, and acceptor density of Cu_2O were found to be 3.2 eV, 60 to 100 $cm^2V^{-1}s^{-1}$, and 10^{18} cm^{-3}, respectively. The simulation findings showed that a matched valance energy band of Cu_2O resulted in improvements in the performance of the PSCs, whereas an unmatched valance energy band of Cu_2O led to a high charge recombination rate and poor device performance. Low work function electrodes impeded charge transport by forming large Schottky barriers; hence, high work function of a metal electrode is needed for a low charge transport barrier. A PCE of 25.2% was attained under optimal conditions, demonstrating that Cu_2O-based PSCs are promising for future applications.

Author Contributions: Formal analysis, I.B.S. and I.M.O.; Funding acquisition, S.A. and I.M.O.; Investigation, S.S.; Methodology, S.S.; Supervision, S.A.; Validation, S.A.; Writing—original draft, S.S.; Writing—review & editing, I.B.S. and I.M.O. All authors contributed to the writing of the manuscript. All authors have read and agreed to the published version of the manuscript.

Data Availability Statement: All the data presented in the manuscript can be obtained from the corresponding author by reasonable request.

Conflicts of Interest: The authors do not have any conflicts of interest to disclose.

References

1. Park, N. Methodologies for high efficiency perovskite solar cells. *Nano Converg.* **2016**, *3*, 15. [CrossRef] [PubMed]
2. Wei, D.; Ma, F.; Wang, R.; Dou, S.; Cui, P.; Huang, H.; Ji, J.; Jia, E.; Jia, X.; Sajid, S.; et al. Ion-Migration Inhibition by the Cation–π Interaction in Perovskite Materials for Efficient and Stable Perovskite Solar Cells. *Adv. Mater.* **2018**, *30*, 1707583. [CrossRef] [PubMed]
3. Kojima, A.; Teshima, K.; Shirai, Y.; Miyasaka, T. Organometal halide perovskites as visible-light sensitizers for photovoltaic cells. *J. Am. Chem. Soc.* **2009**, *131*, 6050–6051. [CrossRef] [PubMed]
4. Im, J.-H.; Lee, C.-R.; Lee, J.-W.; Park, S.-W.; Park, N.-G. 6.5% efficient perovskite quantum-dot-sensitized solar cell. *Nanoscale* **2011**, *3*, 4088–4093. [CrossRef]
5. Kim, H.; Lee, C.; Im, J.; Lee, K.; Moehl, T.; Marchioro, A.; Moon, S.; Humphry-baker, R.; Yum, J.; Moser, J.E.; et al. Lead Iodide Perovskite Sensitized All-Solid-State Submicron Thin Film Mesoscopic Solar Cell with Efficiency Exceeding 9%. *Science* **2012**, *2*, 591. [CrossRef]
6. Kim, G.-H.; Kim, D.S. Development of perovskite solar cells with >25% conversion efficiency. *Joule* **2021**, *5*, 1033–1035. [CrossRef]
7. Kim, G.; Kim, J.; Lee, G.; Kang, G.; Lee, J.; Park, T. A strategy to design a donor–π–acceptor polymeric hole conductor for an efficient perovskite solar cell. *Adv. Energy Mater.* **2015**, *5*, 1500471. [CrossRef]
8. Brauer, J.C.; Lee, Y.H.; Khaja Nazeeruddin, M.; Banerji, N. Charge Transfer Dynamics from Organometal Halide Perovskite to Polymeric Hole Transport Materials in Hybrid Solar Cells. *J. Phys. Chem. Lett.* **2015**, *6*, 3675–3681. [CrossRef]
9. Sajid, S.; Elseman, A.M.; Huang, H.; Ji, J.; Dou, S.; Jiang, H.; Liu, X.; Wei, D.; Cui, P.; Li, M. Breakthroughs in NiOx-HTMs towards stable, low-cost and efficient perovskite solar cells. *Nano Energy* **2018**, *51*, 408–424. [CrossRef]
10. Sajid, S.; Elseman, A.M.; Wei, D.; Ji, J.; Dou, S.; Huang, H.; Cui, P.; Li, M. NiO@carbon spheres: A promising composite electrode for scalable fabrication of planar perovskite solar cells at low cost. *Nano Energy* **2019**, *55*, 470–476. [CrossRef]
11. Sajid; Elseman, A.M.; Ji, J.; Dou, S.; Huang, H.; Cui, P.; Wei, D.; Li, M. Novel hole transport layer of nickel oxide composite with carbon for high-performance perovskite solar cells. *Chin. Phys. B* **2018**, *27*, 17305. [CrossRef]
12. Sajid, S.; Mourtada, A.; Jun, E.; Shangyi, J.; Dong, D.; Hao, W.; Peng, H. Computational Study of Ternary Devices: Stable, Low-Cost, and Efficient Planar Perovskite Solar Cells. *Nano-Micro Lett.* **2018**, *10*, 51. [CrossRef] [PubMed]
13. Chang, C.-Y.; Chang, Y.-C.; Huang, W.-K.; Liao, W.-C.; Wang, H.; Yeh, C.; Tsai, B.-C.; Huang, Y.-C.; Tsao, C.-S. Achieving high efficiency and improved stability in large-area ITO-free perovskite solar cells with thiol-functionalized self-assembled monolayers. *J. Mater. Chem. A* **2016**, *4*, 7903–7913. [CrossRef]
14. Wu, Y.; Zhu, H.; Yu, B.-B.; Akin, S.; Liu, Y.; Shen, Z.; Pan, L.; Cai, H. Interface Modification to Achieve High-efficiency and Stable Perovskite Solar Cells. *Chem. Eng. J.* **2022**, *433*, 134613. [CrossRef]
15. Shaikh, J.S.; Shaikh, N.S.; Mishra, Y.K.; Kanjanaboos, P.; Shewale, P.M.; Sabale, S.; Praserthdam, S.; Lokhande, C.D. Low-cost Cu-based inorganic hole transporting materials in perovskite solar cells: Recent progress and state-of-art developments. *Mater. Today Chem.* **2021**, *20*, 100427. [CrossRef]
16. Elseman, A.M.; Sharmoukh, W.; Sajid, S.; Cui, P.; Ji, J.; Dou, S.; Wei, D.; Huang, H.; Xi, W.; Chu, L.; et al. Superior Stability and Efficiency Over 20% Perovskite Solar Cells Achieved by a Novel Molecularly Engineered Rutin–AgNPs/Thiophene Copolymer. *Adv. Sci.* **2018**, *5*, 1800568. [CrossRef]
17. Elseman, A.M.; Sajid, S.; Shalan, A.E.; Mohamed, S.A.; Rashad, M.M. Recent progress concerning inorganic holetransport layers for efficient perovskite solar cells. *Appl. Phys. A* **2019**, *125*, 476. [CrossRef]
18. Urbina, A. The balance between efficiency, stability and environmental impacts in perovskite solar cells: A review. *J. Phys. Energy* **2020**, *2*, 22001. [CrossRef]
19. Mali, S.S.; Kim, H.; Kim, H.H.; Shim, S.E.; Hong, C.K. Nanoporous p-type NiOx electrode for pin inverted perovskite solar cell toward air stability. *Mater. Today* **2018**, *21*, 483–500. [CrossRef]
20. Christians, J.A.; Fung, R.C.M.; Kamat, P. V An inorganic hole conductor for organo-lead halide perovskite solar cells. Improved hole conductivity with copper iodide. *J. Am. Chem. Soc.* **2014**, *136*, 758–764. [CrossRef]
21. Kim, B.-S.; Kim, T.-M.; Choi, M.-S.; Shim, H.-S.; Kim, J.-J. Fully vacuum–processed perovskite solar cells with high open circuit voltage using MoO_3/NPB as hole extraction layers. *Org. Electron.* **2015**, *17*, 102–106. [CrossRef]
22. Hu, L.; Peng, J.; Wang, W.; Xia, Z.; Yuan, J.; Lu, J.; Huang, X.; Ma, W.; Song, H.; Chen, W. Sequential deposition of CH3NH3PbI3 on planar NiO film for efficient planar perovskite solar cells. *Acs Photonics* **2014**, *1*, 547–553. [CrossRef]
23. Haque, M.A.; Sheikh, A.D.; Guan, X.; Wu, T. Metal oxides as efficient charge transporters in perovskite solar cells. *Adv. Energy Mater.* **2017**, *7*, 1602803. [CrossRef]
24. Lai, W.-C.; Lin, K.-W.; Guo, T.-F.; Chen, P.; Liao, Y.-Y. Perovskite-based solar cells with inorganic inverted hybrid planar heterojunction structure. *AIP Adv.* **2018**, *8*, 15109. [CrossRef]
25. Qin, P.; Tanaka, S.; Ito, S.; Tetreault, N.; Manabe, K.; Nishino, H.; Nazeeruddin, M.K.; Grätzel, M. Inorganic hole conductor-based lead halide perovskite solar cells with 12.4% conversion efficiency. *Nat. Commun.* **2014**, *5*, 3834. [CrossRef]
26. Ansari, F.; Salavati-Niasari, M.; Amiri, O.; Mir, N.; Abdollahi Nejand, B.; Ahmadi, V. Magnetite as inorganic hole transport material for lead halide perovskite-based solar cells with enhanced stability. *Ind. Eng. Chem. Res.* **2020**, *59*, 743–750. [CrossRef]
27. Tirado, J.; Roldán-Carmona, C.; Muñoz-Guerrero, F.A.; Bonilla-Arboleda, G.; Ralaiarisoa, M.; Grancini, G.; Queloz, V.I.E.; Koch, N.; Nazeeruddin, M.K.; Jaramillo, F. Copper sulfide nanoparticles as hole-transporting-material in a fully-inorganic blocking layers nip perovskite solar cells: Application and working insights. *Appl. Surf. Sci.* **2019**, *478*, 607–614. [CrossRef]

28. Akin, S.; Liu, Y.; Dar, M.I.; Zakeeruddin, S.M.; Grätzel, M.; Turan, S.; Sonmezoglu, S. Hydrothermally processed CuCrO$_2$ nanoparticles as an inorganic hole transporting material for low-cost perovskite solar cells with superior stability. *J. Mater. Chem. A* **2018**, *6*, 20327–20337. [CrossRef]

29. Liu, C.; Zhou, X.; Chen, S.; Zhao, X.; Dai, S.; Xu, B. Hydrophobic Cu$_2$O Quantum Dots Enabled by Surfactant Modification as Top Hole-Transport Materials for Efficient Perovskite Solar Cells. *Adv. Sci.* **2019**, *6*, 1801169. [CrossRef]

30. Elseman, A.M.; Selim, M.S.; Luo, L.; Xu, C.Y.; Wang, G.; Jiang, Y.; Liu, D.B.; Liao, L.P.; Hao, Z.; Song, Q.L. Efficient and Stable Planar n-i-p Perovskite Solar Cells with Negligible Hysteresis through Solution-Processed Cu$_2$O Nanocubes as a Low-Cost Hole-Transport Material. *ChemSusChem* **2019**, *12*, 3808–3816. [CrossRef]

31. Würfel, U.; Cuevas, A.; Würfel, P. Charge Carrier Separation in Solar Cells. *IEEE J. Photovoltaics* **2015**, *5*, 461–469. [CrossRef]

32. Karthick, S.; Velumani, S.; Bouclé, J. Experimental and SCAPS simulated formamidinium perovskite solar cells: A comparison of device performance. *Sol. Energy* **2020**, *205*, 349–357. [CrossRef]

33. Kang, A.K.; Zandi, M.H.; Gorji, N.E. Simulation analysis of graphene contacted perovskite solar cells using SCAPS-1D. *Opt. Quantum Electron.* **2019**, *51*, 91. [CrossRef]

34. Bansal, S.; Aryal, P. Evaluation of new materials for electron and hole transport layers in perovskite-based solar cells through SCAPS-1D simulations. In Proceedings of the 2016 IEEE 43rd Photovoltaic Specialists Conference (PVSC), Portland, OR, USA, 5–10 June 2016; pp. 747–750. [CrossRef]

35. Ahmed, S.; Jannat, F.; Khan, M.A.K.; Alim, M.A. Numerical development of eco-friendly Cs$_2$TiBr$_6$ based perovskite solar cell with all-inorganic charge transport materials via SCAPS-1D. *Optik* **2021**, *225*, 165765. [CrossRef]

36. Burgelman, M.; Nollet, P.; Degrave, S. Modelling polycrystalline semiconductor solar cells. *Thin Solid Films* **2000**, *361–362*, 527–532. [CrossRef]

37. Burgelman, M.; Decock, K.; Khelifi, S.; Abass, A. Advanced electrical simulation of thin film solar cells. *Thin Solid Films* **2013**, *535*, 296–301. [CrossRef]

38. Ma, F.; Zhao, Y.; Li, J.; Zhang, X.; Gu, H.; You, J. Nickel oxide for inverted structure perovskite solar cells. *J. Energy Chem.* **2021**, *52*, 393–411. [CrossRef]

39. Chen, Y.-J.; Li, M.-H.; Huang, J.-C.-A.; Chen, P. Cu/Cu$_2$O nanocomposite films as a p-type modified layer for efficient perovskite solar cells. *Sci. Rep.* **2018**, *8*, 7646. [CrossRef]

40. Wang, H.; Yu, Z.; Lai, J.; Song, X.; Yang, X.; Hagfeldt, A.; Sun, L. One plus one greater than two: High-performance inverted planar perovskite solar cells based on a composite CuI/CuSCN hole-transporting layer. *J. Mater. Chem. A* **2018**, *6*, 21435–21444. [CrossRef]

41. Chen, Q.; Ni, Y.; Dou, X.; Yoshinori, Y. The Effect of Energy Level of Transport Layer on the Performance of Ambient Air Prepared Perovskite Solar Cell: A SCAPS-1D Simulation Study. *Crystals* **2022**, *12*, 68. [CrossRef]

42. Aseena, S.; Abraham, N.; Babu, V.S. Simulation Based Investigation on the Performance of Metal Oxides as Charge Transport Layers in Lead/Tin Perovskite Solar Cells Using SCAPS 1D. *ECS J. Solid State Sci. Technol.* **2021**, *10*, 71012.

43. Bisquert, J.; Janssen, M. From frequency domain to time transient methods for halide perovskite solar cells: The connections of IMPS, IMVS, TPC, and TPV. *J. Phys. Chem. Lett.* **2021**, *12*, 7964–7971. [CrossRef]

44. Shao, S.; Liu, J.; Portale, G.; Fang, H.; Blake, G.R.; ten Brink, G.H.; Koster, L.J.A.; Loi, M.A. Highly reproducible Sn-based hybrid perovskite solar cells with 9% efficiency. *Adv. Energy Mater.* **2018**, *8*, 1702019. [CrossRef]

45. Chouhan, A.S.; Jasti, N.P.; Avasthi, S. Effect of interface defect density on performance of perovskite solar cell: Correlation of simulation and experiment. *Mater. Lett.* **2018**, *221*, 150–153. [CrossRef]

46. Sajid, S.; Huang, H.; Ji, J.; Jiang, H.; Duan, M.; Liu, X.; Liu, B.; Li, M. Quest for robust electron transporting materials towards efficient, hysteresis-free and stable perovskite solar cells. *Renew. Sustain. Energy Rev.* **2021**, *152*, 111689. [CrossRef]

47. Elseman, A.M.; Shalan, A.E.; Sajid, S.; Rashad, M.M.; Hassan, A.M.; Li, M. Copper-Substituted Lead Perovskite Materials Constructed with Different Halides for Working (CH$_3$NH$_3$)$_2$CuX$_4$-Based Perovskite Solar Cells from Experimental and Theoretical View. *ACS Appl. Mater. Interfaces* **2018**, *10*, 11699–11707. [CrossRef]

48. Bui, A.D.; Mozaffari, N.; Truong, T.N.; Duong, T.; Weber, K.J.; White, T.P.; Catchpole, K.R.; Macdonald, D.; Nguyen, H.T. Electrical properties of perovskite solar cells by illumination intensity and temperature-dependent photoluminescence imaging. *Prog. Photovolt. Res. Appl.* **2021**, *30*, 1038–1044. [CrossRef]

49. Yang, M.; Zhang, T.; Schulz, P.; Li, Z.; Li, G.; Kim, D.H.; Guo, N.; Berry, J.J.; Zhu, K.; Zhao, Y. Facile fabrication of large-grain CH3NH3PbI3−xBrx films for high-efficiency solar cells via CH$_3$NH$_3$Br-selective Ostwald ripening. *Nat. Commun.* **2016**, *7*, 12305. [CrossRef]

50. Haider, S.Z.; Anwar, H.; Wang, M. Theoretical Device Engineering for High—Performance Perovskite Solar Cells Theoretical Device Engineering for High-Performance Perovskite Solar Cells Using CuSCN as Hole Transport Material Boost the Efficiency Above 25%. *Phys. Status Solidi* **2019**, *216*, 1900102. [CrossRef]

51. Zulqarnain, S.; Anwar, H.; Manzoor, S.; Ismail, A.G.; Wang, M. A theoretical study for high-performance inverted p-i-n architecture perovskite solar cells with cuprous iodide as hole transport material. *Curr. Appl. Phys.* **2020**, *20*, 1080–1089. [CrossRef]

52. Sekkat, A.; Nguyen, V.H.; Masse de La Huerta, C.A.; Rapenne, L.; Bellet, D.; Kaminski-Cachopo, A.; Chichignoud, G.; Muñoz-Rojas, D. Open-air printing of Cu$_2$O thin films with high hole mobility for semitransparent solar harvesters. *Commun. Mater.* **2021**, *2*, 78. [CrossRef]

53. Gong, J.; Krishnan, S. Simulation of Inverted Perovskite Solar Cells. *Energy Sustain.* **2018**, *51418*, V001T12A002. [CrossRef]

54. Adams, G.R.; Obiozo, V.; Shohag, A.S. Simulation of carriers spatial distribution and transportation in co-mixing composition perovskite for solar cell Simulation of carriers spatial distribution and transportation in co-mixing composition perovskite for solar cell. *Mater. Res. Express* **2021**, *8*, 035006. [CrossRef]

55. Hossain, M.I.; Alharbi, F.H.; Tabet, N. Copper oxide as inorganic hole transport material for lead halide perovskite based solar cells. *Sol. Energy* **2015**, *120*, 370–380. [CrossRef]

56. Lin, L.; Jiang, L.; Li, P.; Fan, B.; Qiu, Y. A modeled perovskite solar cell structure with a Cu_2O hole-transporting layer enabling over 20% efficiency by low-cost low-temperature processing. *J. Phys. Chem. Solids* **2019**, *124*, 205–211. [CrossRef]

57. Huang, H.; Liu, X.; Duan, M.; Ji, J.; Jiang, H.; Liu, B.; Sajid, S.; Cui, P.; Wei, D.; Li, Y.; et al. Dual Function of Surface Alkali-Gas Erosion on SnO_2 for Efficient and Stable Perovskite Solar Cells. *ACS Appl. Energy Mater.* **2020**, *3*, 5039–5049. [CrossRef]

58. Kim, S.H.; Park, C.H.; Saeed, M.A.; Ko, D.-H.; Lee, J.-H.; Shim, J.W. b-cyclodextrinepolyacryloyl hydrazide-based surface modification for efficient electron-collecting electrodes of indoor organic photovoltaics. *J. Mater. Res. Technol.* **2022**, *16*, e1666. [CrossRef]

59. Ahsan Saeed, M.; Hyeon Kim, S.; Baek, K.; Hyun, J.K.; Youn Lee, S.; Won Shim, J. PEDOT:PSS: CuNW-based transparent composite electrodes for high-performance and flexible organic photovoltaics under indoor lighting. *Appl. Surf. Sci.* **2021**, *567*, 150852. [CrossRef]

60. Kim, S.; Ahsan Saeed, M.; Hyeon Kim, S.; Won Shim, J. Enhanced hole selecting behavior of WO_3 interlayers for efficient indoor organic photovoltaics with high fill-factor. *Appl. Surf. Sci.* **2020**, *527*, 146840. [CrossRef]

61. Raoui, Y.; Ez-Zahraouy, H.; Kazim, S.; Ahmad, S. Energy level engineering of charge selective contact and halide perovskite by modulating band offset: Mechanistic insights. *J. Energy Chem.* **2021**, *54*, 822–829. [CrossRef]

62. Yu, Z.; Sun, L. Inorganic Hole-Transporting Materials for Perovskite Solar Cells. *Small Methods* **2018**, *2*, 1700280. [CrossRef]

63. Alnuaimi, A.; Almansouri, I.; Nayfeh, A. Effect of mobility and band structure of hole transport layer in planar heterojunction perovskite solar cells using 2D TCAD simulation. *J. Comput. Electron.* **2016**, *15*, 1110–1118. [CrossRef]

64. Shivesh, K.; Alam, I.; Kushwaha, A.K.; Kumar, M.; Singh, S.V. Investigating the theoretical performance of Cs_2TiBr_6-based perovskite solar cell with La-doped $BaSnO_3$ and $CuSbS_2$ as the charge transport layers. *Int. J. Energy Res.* **2022**, *46*, 6045–6064. [CrossRef]

65. Liu, F.; Zhu, J.; Wei, J.; Li, Y.; Lv, M.; Yang, S.; Zhang, B.; Yao, J.; Dai, S. Numerical simulation: Toward the design of high-efficiency planar perovskite solar cells. *Appl. Phys. Lett.* **2014**, *104*, 253508. [CrossRef]

66. Cui, P.; Wei, D.; Ji, J.; Huang, H.; Jia, E.; Dou, S.; Wang, T.; Wang, W.; Li, M. Planar p–n homojunction perovskite solar cells with efficiency exceeding 21.3%. *Nat. Energy* **2019**, *4*, 150–159. [CrossRef]

67. Patel, P.K. Device simulation of highly efficient eco-friendly $CH_3NH_3SnI_3$ perovskite solar cell. *Sci. Rep.* **2021**, *11*, 3082. [CrossRef]

68. Grancini, G.; Roldán-Carmona, C.; Zimmermann, I.; Mosconi, E.; Lee, X.; Martineau, D.; Narbey, S.; Oswald, F.; De Angelis, F.; Graetzel, M. One-Year stable perovskite solar cells by 2D/3D interface engineering. *Nat. Commun.* **2017**, *8*, 15684. [CrossRef]

69. Zhang, H.; Wang, H.; Chen, W.; Jen, A.K. $CuGaO_2$: A promising inorganic hole-transporting material for highly efficient and stable perovskite solar cells. *Adv. Mater.* **2017**, *29*, 1604984. [CrossRef]